Journal of Solid State Chemistry **167,** 517–524 (2002)
doi:10.1006/jssc.2002.9674

New Ternary Compounds $M_xTa_{11-x}Ge_8$ (M=Ti, Zr, Hf): Structure and Stabilization

Klaus W. Richter,*[,1] Hans Flandorfer,* and Hugo F. Franzen†

*Institut für Anorganische Chemie, Universität Wien, Währingerstaße 42, A-1090 Wien, Austria; and †Ames Laboratory and Department of Chemistry, Iowa State University, Ames Iowa, 50011

Received October 7, 2001; in revised form May 9, 2002; accepted May 28, 2002

The title compounds $M_xTa_{11-x}Ge_8$ (M = Ti, Zr, Hf) were prepared from the pure elements by arc-melting and subsequent induction heating at temperatures between 1200°C and 1400°C. X-ray powder diffraction studies of the samples were performed using the Guinier technique and the respective powder patterns were refined with a structure model based on the orthorhombic $Cr_{11}Ge_8$-structure type (*oP*76, *Pnma*). The homogeneity ranges of the compounds were determined to be $0.9 < x < 1.3$ (M = Ti), $0.7 < x < 1.3$ (M = Zr) and $0.7 < x < 2.4$ (M = Hf) by means of electron probe microanalysis. Chemical bonding, electronic structure and site preferences are discussed based on extended Hückel calculations performed on hypothetical binary $Ta_{11}Ge_8$. © 2002 Elsevier Science (USA)

Key Words: **ternary germanides; crystal structure; bonding; disorder; differential fractional site occupation.**

INTRODUCTION

Ternary germanides of the type $M_xM_y'Ge$, where M and M' are two early transition metals (group 4 and 5 of the periodic system) have not been investigated extensively in the past. Due to the similar properties of these metals one might assume that extended solid solutions rather than new ternary compounds will be formed as the main result of the addition of a third transition metal element to a binary M–Ge system. This point of view, however, was not confirmed by our recent study in the Ge–Zr–Ta system, where we could find the two new ternary compounds $Zr_{4-x}Ta_{1+x}Ge_4$ and $Zr_{2+x}Ta_{3-x}Ge_4$, showing fractional site occupancy between Ta and Zr at the metal sites in combination with strong site preferences on different sites (1). Similar structural features (i.e., the variation of the metal-to-metal ratio at different mixed metal sites) have been observed earlier for several ternary sulfides and phosphides like, e.g., mixed Nb–Ta sulfides (2–5), $Hf_{10}Ta_3S_3$ (6) and $Hf_{5.08}Mo_{0.92}P_3$ (7). These observations ultimately led to the concept of the stabilization of partially ordered solid solution phases by *differential fractional site occupancy* (DFSO) (8).

In the current work, we report the preparation and structural characterization of the new ternary compounds $M_xTa_{11-x}Ge_8$ (M = Ti, Zr, Hf) and discuss their electronic structure as well as the fractional site occupancies among the transition metals in the context of the DFSO concept.

EXPERIMENTAL SECTION

Synthesis

The samples were prepared from Ge lump (99.9999%, Alfa AESAR), Ta-foil (99.95%, Alfa AESAR), Hf-foil (99.9%, Ames Lab, IA), Zr-rod (99.99%, Ames Lab, IA) and Ti-rod (99.7%, Alfa AESAR). Calculated amounts of the elements were weighed to an accuracy of 0.05 mg, and arc-melted on a water-cooled copper hearth under an argon atmosphere. The obtained reguli with a total mass of about 1000 mg were remelted two times for homogenization and then weighed back in order to check for possible mass losses. Mass losses of 1–3 weight percent during the arc-melting process were attributed to the evaporation of germanium and were compensated by the addition of extra germanium to the initial sample mixtures. The title compounds are not present in the arc-melted samples which contain a mixture of Mn_5Si_3- and W_5Si_3-type compounds with $TaGe_2$.

For phase formation and equilibration, the reguli were annealed for 24–48 h at 1300°C by induction heating in a tungsten crucible under a dynamic vacuum of $p < 2 \times 10^{-6}$ Torr or alternatively in an alumina crucible inside a graphite susceptor in an Ar atmosphere at a pressure of approximately 2 bar. Alternative sample preparation routes were also tested and included tube furnace annealing at 1200–1400°C for up to 10 days in closed Ta-tubes as well as in sealed and evacuated quartz glass tubes

[1] To whom correspondence should be addressed. Fax: +431-4277-9526. E-mail: richter@ap.univie.ac.at.

0022-4596/02 $35.00

at 1100° for 4 weeks. It was not possible to prepare an isostructural binary compound $Ta_{11}Ge_8$ by any of the mentioned synthetic routes.

The fact, that the title compounds were not found in the samples directly after arc melting indicates that $M_xTa_{11-x}Ge_8$ is formed in a solid state reaction at lower temperatures rather than directly from the liquid phase. The title compounds could be prepared by annealing of the arc-melted reguli at 1200°C, 1300°C and 1400°C, respectively, while annealing experiments at 1100°C did not yield in the formation of the compound. A (presumably eutectoid) decomposition of the phase between 1200°C and 1100°C is thus likely.

The title compounds could be synthesized in high yields (more than 90%), but not entirely pure. This is due to significant germanium losses during arc melting as well as during the annealing procedure. The high evaporation rates for germanium make it difficult to control the germanium to metal ratio of the samples and interfere with the homogenization process during annealing. Various synthesis experiments showed that high yields are obtained by using excess germanium (10–15%) and annealing time of 48 h at 1300°C.

Characterization and Structure Refinement

Powder patterns were obtained with a Guinier-Huber chamber using Cu$K\alpha_1$ radiation and employing an internal standard of high-purity Si for lattice parameter determination. The pattern of the new ternary phase was initially observed in a sample with the nominal composition (in atomic percent) $Ta_{50}Zr_5Ge_{45}$. The observed powder pattern could be indexed orthorhombically and the respective lattice parameters, as well as the intensities of the diffraction lines, were found to agree well with a structure model based on the $Cr_{11}Ge_8$-structure type (*oP*76, *Pnma*).

Samples with varying Ta–*M* ratio were prepared for a systematic investigation of possible homogeneity ranges. In order to determine accurate phase compositions of the title compounds and additional impurity phases, samples annealed at 1300°C for approximately 48 h were investigated with a Cameca SX100 electron microprobe (Cameca, Courbevoie Cedex, France) using wavelength dispersive spectroscopy (WDS) for quantitative analyses and employing high-purity Ge, Ta, Ti, Zr and Hf as standard materials. Measurements were performed at 15 kV acceleration voltage and 20 nA electron beam current using the characteristic $L\alpha$ radiation of Ge, Zr, Hf and Ta and $K\alpha$ of Ti for analysis. The limiting compositions of title compounds were determined to be (in atomic percent) $Ti_5Ta_{54}Ge_{41}$–$Ti_7Ta_{52}Ge_{41}$, $Zr_4Ta_{55}Ge_{41}$–$Zr_7Ta_{52}Ge_{41}$ and $Hf_4Ta_{55}Ge_{41}$–$Hf_{13}Ta_{46}Ge_{41}$, respectively. The metal–germanium ratio determined by EPMA agrees well with the proposed stoichiometry. In terms of the chemical formula $M_xTa_{11-x}Ge_8$, the homogeneity ranges of the compounds may thus be given as $0.9<x<1.3$ (M = Ti), $0.7<x<1.3$ (M = Zr) and $0.7<x<2.4$ (M = Hf). The respective variations of the lattice parameters with the composition from the minimum to the maximum value for x are: a = 14.12(1)–14.15(3) Å, b = 5.311(1)–5.326(1) Å, c = 16.88(2)–16.94(3) Å for $Zr_xTa_{11-x}Ge_8$ and a = 14.12(1)–14.18(1) Å, b = 5.323(1)–5.343(1) Å, c = 16.87(3)–16.97(1) Å for $Hf_xTa_{11-x}Ge_8$. In the case of $Ti_xTa_{11-x}Ge_8$, no significant variation of lattice parameters with the composition was observed. This is consistent with the almost similar size of Ta and Ti.

Various attempts to obtain single crystals suitable for X-ray structure analysis failed due to the fact that the title compounds are not formed directly from the melt, but rather in a solid state reaction at lower temperatures. Even after annealing up to 10 days at 1300°C, no single crystals were observed. It was thus decided to use powder diffraction data for structure refinement. A Guinier-Huber G670 Image Plate System with Cu$K\alpha_1$ radiation was used to record the powder patterns of three ternary samples that were first characterized by EPMA in order to obtain accurate phase compositions. The respective compositions of the title compounds as determined by EPMA are $Ti_{1.1}Ta_{9.9}Ge_8$, $Zr_{1.0}Ta_{10.0}Ge_8$ and $Hf_{2.3}Ta_{8.7}Ge_8$. Rietveld refinement was carried out using the program Fullprof (9). Crystallographic data and refinement parameters for the three samples are listed in Table 1. The impurity phases listed in Table 1 could be refined together with the title compounds without difficulties. As all three compounds are isostructural their atomic parameters do not differ significantly. A full set of atomic parameters is therefore given only for the phase $Hf_{2.3}Ta_{8.7}Ge_8$ (Table 2). A complete list of atomic parameters for all three compounds may be obtained from the corresponding author.

Due to the similarity of the scattering factors of Ta and Hf, a refinement of the site occupation on the *M* positions was not attempted for the compound $Hf_{2.3}Ta_{8.7}Ge_8$ (compare Table 2). In contrast, site occupations on the metal positions could be refined for the compounds $Ti_{1.1}Ta_{9.9}Ge_8$ and $Zr_{1.0}Ta_{10.0}Ge_8$. In order to minimize possible errors introduced by an extensively large set of refinement parameters, the following refinement strategy was used for the refinement. In a first step, metal positions were assumed to be fully occupied with Ta atoms and atomic and profile parameters were refined based on this model. Based on the observed differences in the isotropic displacement parameters of the different metal positions it was possible to identify metal positions requiring less electron density and thus partial filling with Ti or Zr.

In the case of the compound $Zr_{1.0}Ta_{10.0}Ge_8$, the metal position *M*4 showed on unreasonably large isotropic displacement parameter (5.44 Å^2) after refinement as $Ta_{11}Ge_8$. Mixed Zr/Ta occupation was thus allowed for

TABLE 1
Selected Crystal Data and Refinement Parameters for $M_xTa_{11-x}Ge_8$ (M = Ti, Zr, Hf)

Empirical formula[a]	$Ti_{1.1}Ta_{9.9}Ge_8$	$Zr_{1.0}Ta_{10.0}Ge_8$	$Hf_{2.3}Ta_{8.7}Ge_8$
Method		Full-profile Rietveld refinement	
Structure type	$Cr_{11}Ge_8$-type (*oP*76, *Pnma*)		
Lattice parameters (Å)	$a = 14.0698(1)$	$a = 14.1273(1)$	$a = 14.1733(1)$
	$b = 5.28003(4)$	$b = 5.31664(4)$	$b = 5.33778(4)$
	$c = 16.8024(1)$	$c = 16.8947(1)$	$c = 16.9681(2)$
2θ range		23.5–100°	
Number of reflections/parameters	957/97	983/97	897/86
Residual values: R_p/R_{wp}	4.61/5.91	3.87/4.94	4.63/6.04
R_I/R_F	3.63/3.02	2.87/2.30	3.41/2.59
Impurity phases	$TaGe_2$	$TaGe_2$	$TaGe_2$
Space group, structure type	$P6_222$, $CrSi_2$-type	$P6_222$, $CrSi_2$-type	$P6_222$, $CrSi_2$-type
R_I/R_F	3.43/1.98	2.58/1.94	3.27/1.75
	Ta_5Ge_3	Ta_5Ge_3	
Space group, structure type	$P6_3/mcm$, Mn_5Si_3-type	$P6_3/mcm$, Mn_5Si_3-type	
R_I/R_F	4.93/4.09	2.82/2.26	

[a] Corresponding to the composition of the phase measured with EPMA.

*M*4 and Zr was substituted for Ta in steps of 0.1 and later 0.05 until the respective isotropic displacement parameter reached reasonable values. A similar procedure was then used for the metal positions *M*1 and *M*2 that also showed unreasonably large displacement parameters. The final occupation model as listed in Table 3 is the best model that could be observed by changes of the occupation of the *M*-positions in steps of 0.05. It combines reasonable isotropic displacement parameters for all nine metal positions with an overall zirconium content in agreement with the formula $Zr_{1.0}Ta_{10.0}Ge_8$ as determined by EPMA. Only three of the nine possible metal sites show occupation with Zr, i.e., distinct site preferences are found in this compound.

Although site preferences of Ti on the *M* positions should have an even larger effect on the isotropic displacement parameters, the respective differences observed in the case of $Ti_{1.1}Ta_{9.9}Ge_8$ after refinement as $Ta_{11}Ge_8$ were found to be much smaller. A procedure similar to the one described before was used to even out the largest differences of isotropic displacement parameters yielding the final occupation model listed in Table 3, which is again consistent with the formula $Ti_{1.1}Ta_{9.9}Ge_8$ determined by EPMA. In contrast to Zr, Ti was found to be distributed over the different *M* sites in a rather uniform way. The observed differences in the substitution mechanism of Ti and Zr are discussed in the following section.

TABLE 2
Atomic Parameters for $Hf_{2.3}Ta_{8.7}Ge_8$

Atom	Site symmetry	x	y	z	B_{eq} (Å^2)
*M*1[a]	4*c*: .*m*.	0.0688(1)	$\frac{1}{4}$	0.8061(1)	1.65(4)
*M*2[a]	4*c*: .*m*.	0.3716(1)	$\frac{1}{4}$	0.9579(1)	1.54(5)
*M*3[a]	4*c*: .*m*.	0.1325(1)	$\frac{1}{4}$	0.3411(1)	1.62(5)
*M*4[a]	4*c*: .*m*.	0.2510(2)	$\frac{1}{4}$	0.5271(1)	1.94(4)
*M*5[a]	4*c*: .*m*.	0.4495(2)	$\frac{1}{4}$	0.4069(1)	1.63(5)
*M*6[a]	4*c*: .*m*.	0.1244(1)	$\frac{1}{4}$	0.0015(1)	1.79(5)
*M*7[a]	4*c*: .*m*.	0.3067(2)	$\frac{1}{4}$	0.2493(1)	1.27(4)
*M*8[a]	8*d*: 1	0.3659(1)	0.9989(3)	0.6740(1)	1.19(3)
*M*9[a]	8*d*: 1	0.0611(1)	0.0013(3)	0.6220(1)	1.41(3)
Ge1	4*c*: .*m*.	0.2046(3)	$\frac{1}{4}$	0.6933(3)	1.41(12)
Ge2	4*c*: .*m*.	0.4186(3)	$\frac{1}{4}$	0.8022(3)	1.57(11)
Ge3	4*c*: .*m*.	0.0541(3)	$\frac{1}{4}$	0.4823(2)	1.19(9)
Ge4	4*c*: .*m*.	0.4547(4)	$\frac{1}{4}$	0.5592(3)	2.12(11)
Ge5	4*c*: .*m*.	0.2743(4)	$\frac{1}{4}$	0.0934(3)	1.81(13)
Ge6	4*c*: .*m*.	0.4886(3)	$\frac{1}{4}$	0.2540(3)	1.41(11)
Ge7	8*d*: 1	0.2143(2)	0.0064(6)	0.8885(2)	1.47(7)

[a] Ta/Hf occupation not refined.

TABLE 3
Proposed Site Occupation Models for $Ta_{9.9}Ti_{1.1}Ge_8$ and $Ta_{10.0}Zr_{1.0}Ge_8$

		$Ti_{1.1}Ta_{9.9}Ge_8$		$Zr_{1.0}Ta_{10.0}Ge_8$	
Position	Site symmetry	Site occupation	B_{eq} (Å^2)	Site occupation	B_{eq} (Å^2)
*M*1	4*c*: *.m.*	0.95 Ta + 0.05 Ti	1.74(4)	0.85 Ta + 0.15 Zr	1.88(5)
*M*2	4*c*: *.m.*	0.85 Ta + 0.15 Ti	1.72(5)	0.75 Ta + 0.25 Zr	1.95(5)
*M*3	4*c*: *.m.*	0.90 Ta + 0.10 Ti	1.56(5)	Ta	2.06(5)
*M*4	4*c*: *.m.*	0.85 Ta + 0.15 Ti	1.83(4)	0.40 Ta + 0.60 Zr	2.01(6)
*M*5	4*c*: *.m.*	0.90 Ta + 0.10 Ti	2.03(5)	Ta	2.21(5)
*M*6	4*c*: *.m.*	0.85 Ta + 0.15 Ti	1.93(5)	Ta	2.12(5)
*M*7	4*c*: *.m.*	Ta	1.97(4)	Ta	1.72(4)
*M*8	8*d*: 1	Ta	1.75(3)	Ta	1.54(3)
*M*9	8*d*: 1	0.80 Ta + 0.20 Ti	1.84(3)	Ta	1.99(3)

Band Structure Calculations

Extended Hückel Calculations were performed using the Caesar program package (10). As the ternary compounds exhibit compositions very close to binary $Ta_{11}Ge_8$, the calculations were performed on hypothetical binary $Ta_{11}Ge_8$ using the refined atomic positions of $Hf_{2.3}Ta_{8.7}Ge_8$ listed in Table 2. The Hückel parameters (orbital energies and Slater coefficients) were taken from previous calculations for the compounds $Zr_{4-x}Ta_{1+x}Ge_4$ and $Zr_{2+x}Ta_{3-x}Ge_4$ (1) and are listed in Table 4.

RESULTS AND DISCUSSION

Crystal Structure

The $Cr_{11}Ge_8$ structure type was first discovered in the compounds $M_{11}Ge_8$ (M = V, Cr, Mn) by Israiloff *et al.* (11). Besides the binary compounds, the ternary silicides $(Nb, Ta)_{11}Si_8$, $(Cr, Ta)_{11}Si_8$ and $(Mn, Mo)_{11}Si_8$ have been reported to crystallize in the same structure type (12). Isotypic antimonides with the composition $(Zr, V)_{11}Sb_8$ (13) and $Ti_{11}(Sb,Sn)_8$ (14) have been reported recently.

A view of the structure along the (short) *b*-axis of $M_xTa_{11-x}Ge_8$ is shown in Fig. 1. The metal atoms are shown in dark gray, while the germanium atoms are drawn as white circles. The graph emphasizes the metal–metal framework (gray bonds) while—for reasons of clarity—the germanium–metal bonds are not shown in the figure. It was already pointed out by Steinmetz *et al.* (12) that the structure can be derived by a combination of fragments of the tetragonal W_5Si_3-type with hexagonal Mn_5Si_3-type fragments. This point is shown in detail in Fig. 2. Distorted Mn_5Si_3-type units within the orthorhombic structure of $M_xTa_{11-x}Ge_8$ are shown in Fig. 2a. The units are interconnected by columns of Ge7 atoms (Table 2). It should be pointed out that the positions of the Ge7 atoms (forming linear chains along the *b*-axis of the orthorhombic unit cell) are not occupied in the basic

TABLE 4
Parameters Used in the Extended Hückel Calculations

Orbital	H_{ii} (eV)	ζ_1	c_1	ζ_2	c_2
Zr, 5*s*	−7.426	1.817			
Zr, 5*p*	−4.740	1.776			
Zr, 4*d*	−8.158	3.835	0.6213	1.505	0.5769
Ta, 6*s*	−8.964	2.280			
Ta, 6*p*	−5.243	2.241			
Ta, 5*d*	−8.537	4.762	0.6815	1.938	0.6815
Ge, 4*s*	−16.00	2.160			
Ge, 4*p*	−9.00	1.850			

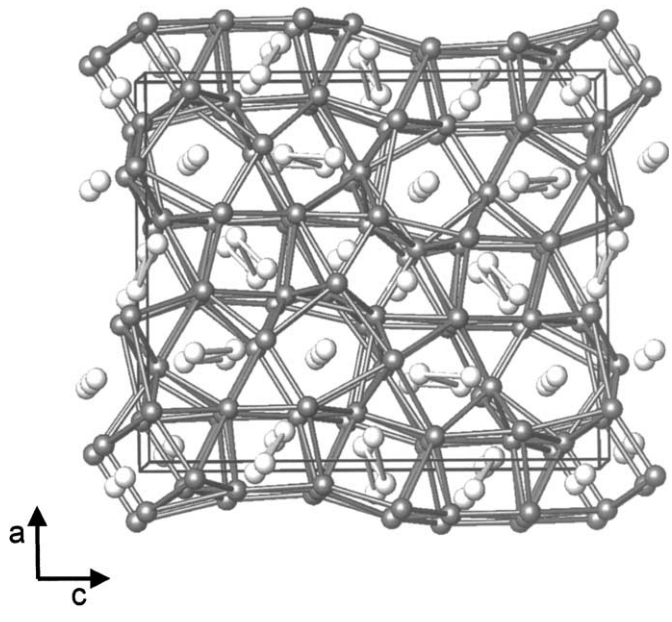

FIG. 1. The crystal structure of $M_xTa_{11-x}Ge_8$ (M = Ti, Zr, Hf); view along [010]. Gray spheres: metal atoms; bright spheres: germanium atoms. Metal–metal bonds are given in gray, Ge–Ge interactions in white.

Mn_5Si_3 structure. The filled variant of this structure type is known as Ti_5Ga_4 structure type. The distortion of the unit relative to the hexagonal parent cell is only moderate: the Ge7–Ge7 distances within the (010) plane (analogous to the *a*- and *b*-axis of the hexagonal unit cell) are 8.50 and 8.54 Å, respectively, while the angle between the atoms is 130.4°. The Mn_5Si_3-type units shown in Fig. 2a are formed by the atoms *M*1–*M*4, *M*7, *M*9, Ge1–Ge3 and Ge5–Ge7 listed in Table 2.

The second sort of building blocks in the structure $M_xTa_{11-x}Ge_8$ is shown in Fig. 2b. These are distorted primitive subunits of the tetragonal W_5Si_3-type structure. These units are formed by the atoms *M*5, *M*6, *M*8, Ge4 and Ge7 (Table 2). The distortion of the unit relative to the tetragonal parent subunit is small: the distances between Ge7 and Ta8 within the (010) plane are 4.98 and 5.05 Å, respectively, and the angle between the atoms is 91.1°. The two building blocks shown in Fig. 2 share the Ge7 atoms forming infinite linear Ge-columns along the *b*-axis of the orthorhombic structure.

The analogy between the building blocks of the orthorhombic structure and the W_5Si_3 and Mn_5Si_3 structure types is useful for the classification and rationalization of the structure, and it should be pointed out that the parent structure types W_5Si_3 and Mn_5Si_3 are very common among early transition metal germanides and both structures have been reported to exist in the binary Ge–Ta system (15). Nevertheless, the structural relations should not be overemphasized. Due to the interconnection of the different building blocks within the metal framework shown in Fig. 1, the local coordination of most atoms in the $Cr_{11}Ge_8$-structure differs from the coordination adopted in the respective parent structure. This is especially true for those atoms located at the border of the building blocks shown in Fig. 2. Only three out of the 16 atomic positions of the orthorhombic structure (as listed in Table 2) show exactly the same type of coordination as they adopt in the parent structure. These are the atoms *M*2, *M*9 and Ge3 in Table 2 that form the NiAs-like columns in the center of the hexagonal Mn_5Si_3-type fragments.

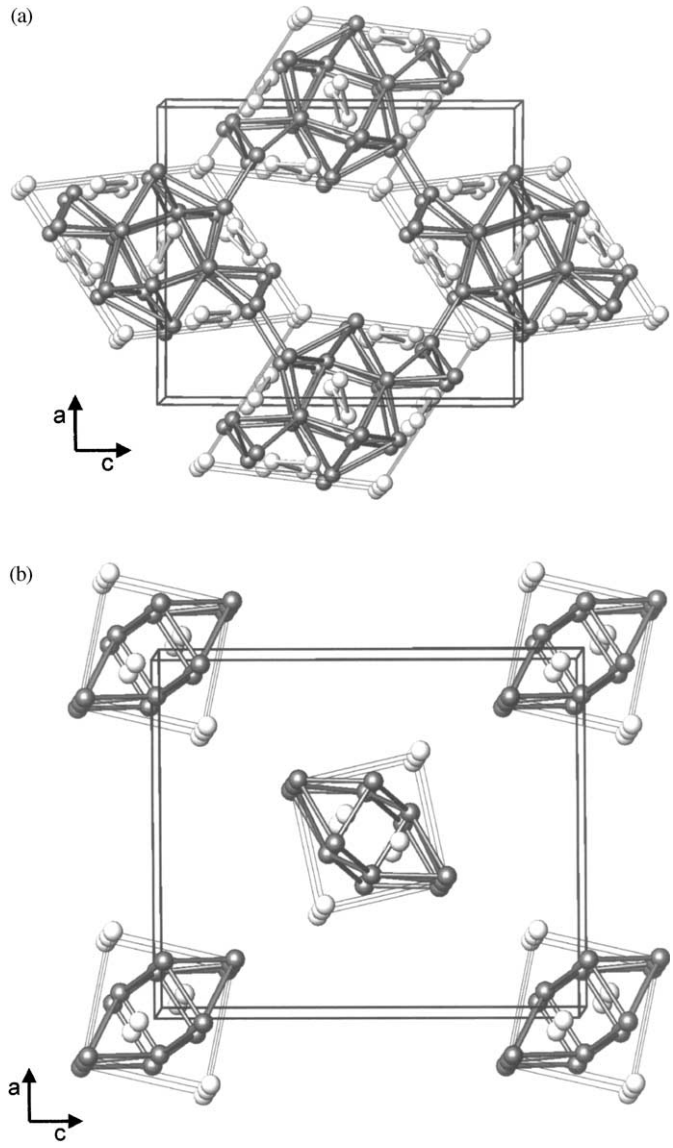

FIG. 2. Building blocks within the crystal structure of $M_xTa_{11-x}Ge_8$. (a) Mn_5Si_3 type units, (b) subunits of the W_5Si_3 type.

Electronic Structure

The density of states, as obtained by extended Hückel calculations, is shown in Fig. 3 together with the respective germanium- and metal-contributions. The Fermi level shown as a dotted line in Fig. 3 corresponds to the composition $M_1Ta_{10}Ge_8$ (344 electrons per unit cell) which is actually part of the composition range in all three compounds discussed here. The lower parts of the DOS curve are dominated by Ge *s*-states and show considerable mixing with Ta-states corresponding to Ta–Ge bonding levels. An analysis of the local density of states shows that the main part of the Ge *s*-block (approximately −19 to

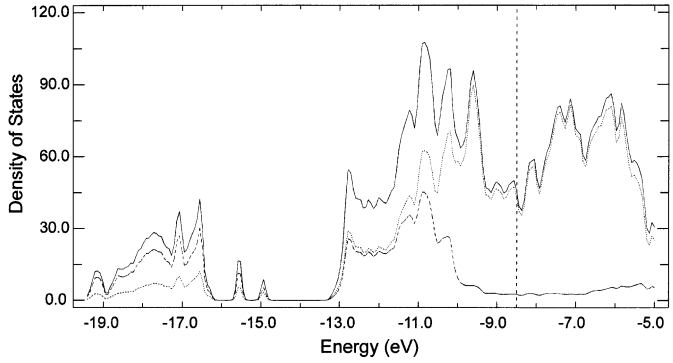

FIG. 3. Density of states for $Cr_{11}Ge_8$-type $Ta_{11}Ge_8$. The Fermi level shown corresponds to the composition $M_{1.0}Ta_{10.0}Ge_8$. Total DOS: solid line, Ta-DOS: dotted line, Ge-DOS: dashed line.

−16 eV) shows contributions from all Ge positions, whereas the two small separated peaks around −15 eV correspond only to the *s*-states of Ge7 which forms the linear chains along the *b*-axis of the orthorhombic unit cell (compare Fig. 1). A gap of approximately 1.5 eV separates these bands from the broad *p*- and *d*-block. While the energetically lower part of this block shows extended mixing of the Ge *p*-states with Ta *s*- and *p*-states, the energetically higher parts of the band near the Fermi level at −8.50 eV are dominated by the *d*-states of Ta. This corresponds to the delocalized metal–metal bonding within the extended metal framework of the structure as emphasized in Fig. 1. The high total density of states at the Fermi level strongly suggests the metallic character of the compound. Due to the high density of states at the Fermi level, changes in the number of electrons (corresponding to a change in the metal/metal ratio) within the homogeneity range do not have a large effect on the Fermi energy.

Strong metal–germanium interactions as well as delocalized metal–metal bonding within the metallic framework are the main contributions to chemical bonding in the compounds $M_xTa_{11-x}Ge_8$ (M = Ti, Zr, Hf). This is reflected by the high-positive cumulated crystal orbital overlap populations (COOP curves) for Ta–Ge and Ta–Ta shown in Fig. 4. Besides these principal contributions, however, some Ge–Ge bonding interactions are also present. A detailed investigation of the local overlap populations reveals that considerable Ge–Ge bonding is only found within the linear chains formed by Ge7 along the *b*-axis of the orthorhombic cell (compare Fig. 1). The respective average overlap population of 0.24 electrons per bond corresponds to the relatively short Ge–Ge distances of 2.59 and 2.73 Å (single bond distance in pure Ge: 2.45 Å) within the linear columns. In contrast, bonding interactions of the various Ge–Ge zig–zag chains within the Mn_5Si_3-type units of the structure (compare Figs. 1 and 2) are almost negligible. Average overlap populations of 0.04 electrons per bond correspond to comparable large Ge–Ge distances (3.11–3.16 Å) within the chains. While the bonding interactions within the Ge–Ge chains occur well below the Fermi level and are partially compensated by antibonding contributions at higher energies, the metal–metal and metal–germanium interactions are of bonding character up to the Fermi level. In fact, metal–metal bonding, as well as metal–germanium bonding, are not optimized for the ternary compounds, i.e., there are still bonding states available at the Fermi level (compare Fig. 4). This is due to the substitution of parts of the group 5 element Ta by the group 4 elements Ti, Zr, Hf yielding in a decrease of the total number of electrons in the unit cell. However, as binary $Ta_{11}Ge_8$ does not exist, this substitution is essential for stabilization of the ternary compound. Fractional site occupations, as they are discussed in the following section, play an important role for the stabilization of the ternary compounds.

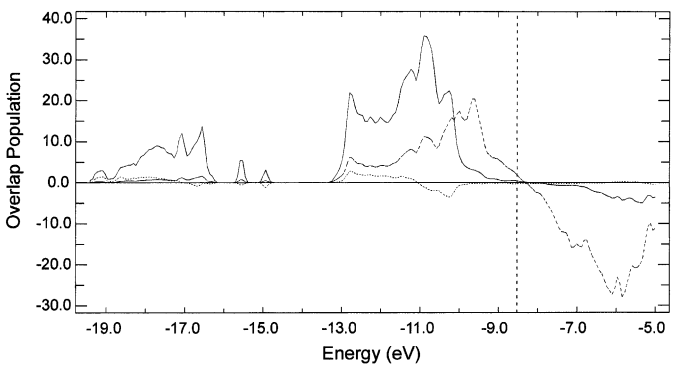

FIG. 4. COOP. Positive values: bonding; negative values: antibonding; Ta–Ge (solid), Ta–Ta (dashed), Ge–Ge (dotted).

Site Occupation

In the simplest case, mixed site occupation would mean a completely random distribution of the group 4 metal atoms over all 9 metal positions of the $Cr_{11}Ge_8$ structure type. This type of mixed site occupation (corresponding to a conventional solid solution) would maximize the stabilizing effect of the configuration entropy term S_{conf} to the Gibbs energy $G = H - TS$. According to the DFSO concept (8), however, differences in the bonding capability between different metals stand against a completely random distribution of the metals and yield site preferences. If both competing factors are balanced, the compound exhibits differential fractional site occupancies, i.e., mixed site occupancies on the metal sites in combination with a pronounced variation of the metal ratio at independent metal sites.

The experimentally observed site occupations in $Ti_{1.1}Ta_{9.9}Ge_8$ and $Zr_{1.0}Ta_{10.0}Ge_8$ listed in Table 3 reveal distinct differences between the Ti- and Zr-containing compounds. Zirconium shows clear preference for only three of the nine independent metal sites ($M1$, $M2$ and $M4$). $Zr_xTa_{11-x}Ge_8$ thus shows DFSO-like behavior similar to the compounds $Zr_{4-x}Ta_{1+x}Ge_4$ and $Zr_{2+x}Ta_{3-x}Ge_4$ reported previously (1). In contrast, the compound $Ti_xTa_{11-x}Ge_8$ does not exhibit pronounced site preferences among different independent sites and Ti was found to be distributed over the different metal sites in a rather uniform way.

A first approach to understand the observed site occupancies in mixed Nb–Ta sulfides was outlined by Yao *et al.* (16), who successfully correlated the cumulated Pauling bond order of a site (as a measure of metal–metal interactions) with the observed site occupancy. It was found that Ta preferably occupied metal sites with higher metal–metal interaction, which was attributed to the larger and more diffuse character of the 5*d* orbitals of Ta with

respect to the 4*d* orbitals of Nb. In a more quantitative approach, Mulliken overlap populations (MOP) obtained by extended Hückel calculations may be used instead of Pauling bond orders as a measure of metal–metal interactions (17).

Niobium and Tantalum, however, are a very special combination of elements, as they are essentially similar in terms of their size (single bond radii according to Pauling (18): 134 pm) as well as in terms of their electronegativity (1.2 for Nb and 1.3 for Ta, respectively). For element pairs that are not related so closely, size effects may play an important role and should be considered in addition to metal–metal bonding arguments based on overlap populations. A different approach, considering differences in electronegativity, has been reviewed recently by Miller (19). In this approach, one uses atomic orbital populations (AOP) obtained by extended Hückel calculations to predict possible site preference effects. The element with the higher electronegativity will preferably occupy the site with the higher atomic orbital population (which therefore may be called "site potential"). As site potentials are calculated on a (hypothetical) homonuclear structure (e.g., $Ta_{11}Ge_8$ instead of $ZrTa_{10}Ge_8$), this approach is simpler to use than an overlap population analysis. Both approaches, MOP as well as AOP analysis, have been successfully used to understand site preferences in the ternary compounds $Zr_{4-x}Ta_{1+x}Ge_4$ and $Zr_{2+x}Ta_{3-x}Ge_4$ (1) and have recently been used to discuss different site occupancy trends in $(M, M')_{21}S_8$ (M, M' = Hf, Ti or Nb, Ta) (20).

The site potential approach together with size considerations may be used for a qualitative discussion of the different site occupation behavior of $Zr_{1.0}Ta_{10.0}Ge_8$ and $Ti_{1.1}Ta_{9.9}Ge_8$. AOP for the different M positions as obtained from extended Hückel calculations on hypothetical $Ta_{11}Ge_8$ are listed in Table 5 together with the site volumes here represented as Dirichlet domains (Voronoi polyhedra) which were calculated using the program Dido by Koch and Fischer (21).

TABLE 5
Atomic Orbital Populations and Dirichlet Domains for $M_xTa_{11-x}Ge_8$

Position	Site symmetry	Total site AOP	Dirichlet domain (Å^3)	Coordination number
*M*1	4*c*: .*m*.	4.57	17.99	16
*M*2	4*c*: .*m*.	4.53	18.00	16
*M*3	4*c*: .*m*.	4.98	16.76	14
*M*4	4*c*: .*m*.	4.50	18.87	17
*M*5	4*c*: .*m*.	4.93	17.70	15
*M*6	4*c*: .*m*.	4.88	17.60	15
*M*7	4*c*: .*m*.	4.94	17.10	14
*M*8	8*d*: 1	5.17	16.34	14
*M*9	8*d*: 1	4.82	16.08	14

In case of the compound $Zr_{1.0}Ta_{10.0}Ge_8$, the site potential approach predicts that the more electropositive metal Zr will preferably occupy the metal sites with the lowest atomic orbital populations. Actually, the metal sites *M*1, *M*2 and *M*4 (which are the only sites that were found to exhibit mixed Ta/Zr site occupation) are the sites with the lowest AOP values. Basic size considerations lead to similar conclusions: as the size of Ta and Zr differ noticeably (single bond radii according to Pauling (18) Ta = 134 pm, Zr = 145 pm), the larger Zr atoms should prefer the higher coordinated sites with larger average contacts to the neighboring atoms. According to the values listed in Table 5, the sites *M*1, *M*2 and *M*4 also show the largest Dirichlet domains of all metal sites.

Ta and Ti, on the other hand, are almost similar in terms of their electronegativity (1.3) as well as in terms of their size (134 and 132 pm, respectively). It is thus consistent with the site potential approach as well as with size considerations, that the compound $Ti_{1.1}Ta_{9.9}Ge_8$ does not show distinct site preferences for Ti.

As mentioned previously, we are not able to propose an occupation model based on X-ray diffraction data for $Hf_{2.3}Ta_{8.7}Ge_8$. However, since Hf and Zr are very similar in size and electronegativity, DFSO-like behavior similar to $Zr_{1.0}Ta_{10.0}Ge_8$ appears to be likely for the Hf-compound. Based on atomic orbital population analysis, we thus predict that Hf preferably occupies the *M*1, *M*2 and *M*4 site of the structure. As the compositional variability of $Hf_xTa_{11-x}Ge_8$ is higher than in the Zr- and Ti analogs, an almost ordered variant of the structure, with *M*1, *M*2 and *M*4 essentially filled up with Hf may be possible at high Hf-contents.

ACKNOWLEDGMENTS

Klaus Richter thanks the Austrian Science Foundation (FWF) for an Erwin-Schrödinger-Scholarship (J1557-CHE). This research was supported by the Office of the Basic Energy Science, US Department of Energy. The Ames Laboratory is operated by the DOE under Contract No. W-7405-Eng-82. The authors thank Peter Rogl and Franz Weitzer for the diffraction measurements with the image plate system.

REFERENCES

1. K. W. Richter and H. F. Franzen, *J. Solid State Chem.* **150,** 347 (2000).
2. X. Yao and H. F. Franzen, *Z. Anorg. Allg. Chem.* **598,** 353 (1991).
3. X. Yao and H. F. Franzen, *J. Solid State Chem.* **86,** 88 (1990).
4. X. Yao and H. F. Franzen, *J. Amer. Chem. Soc.* **113,** 1426 (1991).
5. X. Yao, G. J. Miller, and H. F. Franzen, *J. Alloys Comp.* **183,** 7 (1991).
6. G. A. Marking and H. F. Franzen, *J. Am. Chem. Soc.* **115,** 6126 (1993).

7. J. Cheng and H. F. Franzen, *J. Solid State Chem.* **121,** 362 (1996).
8. H. F. Franzen and M. Köckerling, *Prog. Solid State Chem.* **23,** 265 (1995).
9. J. Rodriguez-Carvajal, "Programme FullProf." Laboratoire Leon Brillouin, France, 1996.
10. J. Ren, W. Liang, and M.-H. Whangbo, "CAESAR Software." North Carolina State University, NC, 1998.
11. P. Israiloff, H. Völlenkle, and A. Wittmann, *Monatsh. Chem.* **105,** 1387 (1974).
12. J. Steinmetz, B. Malaman, and B. Roques, *J. Less-Common Met.* **57,** 133 (1978).
13. H. Kleinke, *J. Mater Chem.* **9,** 2703 (1999).
14. H. Kim, M. M. Olmstead, J. Y. Chan, P. C. Canfield, I. R. Fisher, R. W. Henning, A. J. Schulz, and S. M. Kauzarich, *J. Solid State Chem.* **157,** 225 (2001).
15. P. Villars and L. D. Calvert (Eds.) "Pearsons Handbook of Crystallographic Data for Intermetallic Phases." 2nd ed. ASM, New York, 1991.
16. X. Yao, G. Marking, and H. F. Franzen, *Ber. Bunsenges. Phys. Chem.* **96,** 1552 (1992).
17. M. Köckerling and H. F. Franzen, *Croat. Chem. Acta* **68,** 709 (1995).
18. L. Pauling, "The Nature of the Chemical Bond." Cornell University Press, NY, 1948.
19. G. J. Miller, *Eur. J. Inorg. Chem.* (5), 523 (1998).
20. M. Köckerling and E. Canadell, *Inorg. Chem.* **39,** 4200 (2000).
21. E. Koch and W. Fischer, *Z. Kristallogr.* **211,** 251 (1996).